Relative fragmentation in ternary systems within the temperature-dependent relativistic mean-field approach

M. T. Senthil Kannan,[1,*] Bharat Kumar,[2,3] M. Balasubramaniam,[1] B. K. Agrawal,[3,4] and S. K. Patra[2,3,†]

[1]*Department of Physics, Bharathiar University, Coimbatore 641046, India*

[2]*Institute of Physics, Sachivalaya Marg, Bhubaneswar 751005, India*

[3]*Homi Bhabha National Institute, Anushakti Nagar, Mumbai 400094, India*

[4]*Saha Institute of Nuclear Physics, 1/AF, Bidhannagar, Kolkata 700064, India*

(Received 30 November 2016; revised manuscript received 15 May 2017; published 22 June 2017)

For the first time, we apply the temperature-dependent relativistic mean-field (TRMF) model to study the ternary fragmentation of heavy nuclei using the level density approach. The relative fragmentation probability of a particular fragment is obtained by evaluating the convolution integrals that employ the excitation energy and the level density parameter for a given temperature calculated within the TRMF formalism. To illustrate, we have considered the ternary fragmentations in ^{252}Cf, ^{242}Pu, and ^{236}U with a fixed third fragment $A_3 = {}^{48}$Ca, ^{20}O, and ^{16}O, respectively. The relative fragmentation probabilities are studied for the temperatures $T = 1$, 2, and 3 MeV. For the comparison, the relative fragmentation probabilities are also calculated from the single-particle energies of the finite range droplet model (FRDM). In general, the larger phase space for the ternary fragmentation is observed indicating that such fragmentations are most probable ones. For $T = 2$ and 3 MeV, Sn + Ni + Ca is the most probable combination for the nucleus ^{252}Cf. However, for the nuclei ^{242}Pu and ^{236}U, the maximum fragmentation probabilities at $T = 2$ MeV differ from those at $T = 3$ MeV. For $T = 3$ MeV, the closed shell ($Z = 8$) light-mass fragment with its corresponding partners has larger scission point probabilities. But, at $T = 2$ MeV, Si, P, and S are favorable fragments with the corresponding partners. It is noticed that the symmetric binary fragmentation along with the fixed third fragment for ^{242}Pu and ^{236}U is also favored at $T = 1$ MeV.

DOI: 10.1103/PhysRevC.95.064613

I. INTRODUCTION

The exotic decay modes other than basic decay modes of heavy nuclei need to be studied to understand the reaction kinematics and the structure as well. One such exotic fission mode of heavy nuclei is the splitting into three charged fragments, so-called ternary fission. After earlier reports on ternary fission [1,2], extensive experimental studies on the heavy nuclei ^{252}Cf, ^{242}Pu, and ^{236}U were reported [3–6]. The observations indicate that α particles have the larger yield values. Köster *et al.* [5] reported the ternary fission yields of ^{242}Pu for the various third fragment isotopes up to ^{30}Mg. Pyatkov *et al.* [6,7] reported the ternary fission yields of ^{252}Cf (sf) and ^{236}U ($n_{\rm th}$, f) using the missing mass approach. Sn + Ni/Ge + Ca/S are the most favorable combinations. But theoretically, Fong [8] calculated the probability of α-particle-accompanied fission using statistical theory. Diehl *et al.* [9] applied the liquid drop model to study true ternary fission (TTF) where the three fragments are almost equal by direct prolate/oblate and cascade ternary fission modes. The authors reported that the prolate fission mode is energetically more favorable than the oblate fission mode. Rubchenya and Yavshits [10] applied the dynamical model for ternary fission and reported the formation of light-charged particle at the later descent stage from the saddle point to the scission point. Oertzen and Nasirov [11] obtained the TTF fragments using the potential energy surface calculations. Manimaran and Balasubramaniam [12] proposed the three-cluster model (TCM) to study the α-particle ternary fission and the obtained relative yields are very well in agreement with the experimental data. Further, the TCM was applied to the study of equatorial and collinear configuration [13] of all possible third fragments. The collinear configuration is more favorable for the heavy third particle accompanied fission with the third fragment at the middle of two fragments. Very recently, Karpov [14] applied the three-center shell model to study the potential energy landscape of the ternary fission of ^{252}Cf. The potential energy valleys are favorable for doubly magic Sn as one of the favorable fragments with two other magic or semimagic fragments. Further, Vijayaraghavan *et al.* [15] reported the kinetic energies of ^{252}Cf in a sequential decay mode calculation. Holmvall *et al.* [16] reported the possible kinetic energies in collinear cluster tripartition (CCT) using the true ternary decay mode and studied the stability of collinearity using the Monte Carlo method. That the kinetic energy of the third fragment is almost zero in CCT was reported in Refs. [15,16]. In addition, the intrinsic instability in the collinearity due to the repulsion between the second and third fragments was reported in Ref. [16].

Rajasekaran and Devanathan [17] applied statistical theory to study the binary mass distributions using the single-particle energies of the Nilsson model. The obtained results were well in agreement with the experimental data. As the sequel of this work, Balasubramaniam *et al.* [18] studied the ternary mass distribution of ^{252}Cf for the fixed third fragment ^{48}Ca using the single-particle energies of the finite range droplet model (FRDM) and obtained Sn + Ni + Ca as the most favorable combination at $T = 2$ MeV. Further, the authors

*senthilthulasiram@gmail.com

†patra@iopb.res.in

extended [19] the study to calculate the ternary charge distribution of potential-energy-minimized possible fragments whose probabilities were calculated using the convolution integrals. The results indicate that the most favorable combination has Sn as one of its fragments for temperature $T = 2$ MeV. The excitation energies and the level density parameters for the different fission fragments required to evaluate the convolution integrals in such calculations were obtained using temperature-independent single-particle energies from the FRDM corresponding to the ground-state deformations. The temperature dependence was incorporated through the Fermi-Dirac distributions.

Single-particle energies are usually sensitive to temperature in heavy nuclei, in particular, due to the transition from the deformed to the spherical shape and the transition from the pairing phase to the normal phase as induced by temperature. Such features can significantly affect the temperature dependence of the excitation energy and the level density parameter. The temperature-induced effects on the nuclear deformation and the pairing phase can be readily accounted for within the temperature-dependent nonrelativistic and relativistic mean-field models in a self-consistent manner. Of the main focus in the present investigation is the relativistic mean-field models (RMF). The RMF models at zero temperature [20–24] with various parameter sets have successfully reproduced the bulk properties, such as binding energies, root-mean-square radii, quadrupole deformation, etc., not only for nuclei near the β-stability line but also for nuclei away from it. The temperature-dependent relativistic mean-field (TRMF) model has been employed to study the structural properties of the highly excited hot nuclei [25]. The heavy and rare earth nuclei are studied within the TRMF model [26,27], which indicates that there is a phase transition from the pairing phase to the normal phase around the temperature $T \sim 0.8$ MeV and a shape transition from a prolate shape to a spherical shape at critical temperature $T_c \sim 2.7$ MeV.

The RMF formalism is successfully applied to the study of clusterization of the known cluster emitting heavy nuclei [28–30]. The presence of α clusters in light nuclei, such as ^{12}C, which is also an experimental fact, is explained very convincingly within the framework of the RMF approximation. In addition, it is claimed that the $N \neq Z$ clusters exit in the excited states of heavy nuclei. For superheavy nuclei, the existence of $N \approx Z$ matter is predicted by this theory. The ternary cluster decay from the hyper-hyper deformed ^{56}Ni at high angular momenta that is formed in the ^{32}S + ^{24}Mg reaction is reported in Ref. [31]. The RMF model predicted the two multiple $N = Z$, α-like clusters or the symmetric fission mode of a hyper-hyper deformed ^{56}Ni nucleus [32], which is in contradiction with the experimental results. However, the multiple α-nucleus clusterization is in agreement with earlier experiments. Rutz *et al.* [33] reproduced the double- and triple-humped fission barrier of ^{240}Pu and ^{232}Th and the asymmetric ground states of ^{226}Ra using the RMF formalism. Moreover, the symmetric and asymmetric fission modes have also been successfully reproduced. Patra *et al.* [34] studied the neck configuration in the fission decay of neutron-rich U and Th isotopes. Further, various decay modes, such as α decay, β decay, and cluster decays, are studied in Refs. [35–39] using the RMF formalism with double-folding M3Y, LR3Y, and NLR3Y nucleon-nucleon interaction potential within the preformed cluster model.

In the present work we study the ternary fragmentation of the heavy nuclei ^{252}Cf, ^{242}Pu, and ^{236}U using the TRMF model. The various inputs, like single-particle energies, excitation energies, and the level density parameters of the fission fragments, are calculated using the TRMF model with the well-known NL3 parameter set [40]. For comparison, we calculate the ternary fragmentations using the single-particle energies of the FRDM as explained in Ref. [19].

The article is organized as follows. Section II provides a brief description of statistical theory and the TRMF model with inclusion of the BCS pairing formalism used for this study. In Sec. III we discuss the ternary fragmentation of heavy nuclei and the temperature dependence of the level density parameter and the level density. The main results are summarized in Sec. IV.

II. FORMALISM

We generate different combinations of ternary fission fragments by considering their charge-to-mass ratio to be equal to that of the parent nucleus [17,18], i.e.,

$$\frac{Z_P}{A_P} \approx \frac{Z_i}{A_i}, \tag{1}$$

where A_P and Z_P and A_i and Z_i ($i = 1$, 2, and 3) correspond to the mass and charge numbers of the parent nucleus and the three fission fragments, respectively. The following constraints, $A_1 + A_2 + A_3 = A$, $Z_1 + Z_2 + Z_3 = Z$, and $A_1 \geqslant A_2 \geqslant A_3$ are imposed to satisfy the conservation of mass and charge numbers in the nuclear reaction and to avoid the repetition of fragment combinations. The third fragment A_3 is also considered *a priori* to find the other two fragments A_1 and A_2.

A. Statistical theory

According to statistical theory [17,19,41,42], the ternary fission probability $P(A_j, Z_j)$ is proportional to the folded densities $\rho_{123}(A_j, Z_j, E^*)$ of the three distinct fragments and is given by

$$\rho_{123}(A_j, Z_j, E^*) = \int_0^{E^*} \rho_1(A_1, Z_1, E_1^*) \times \left[\int_0^{E^*} \int_0^{E^*} \prod_{i=2}^{3} \rho_i(A_i, Z_i, E_i^*) \delta[E_2^* + E_3^* - (E^* - E_1^*)] dE_i^* \right] dE_1^*, \tag{2}$$

with E_i^* as the excitation energy. Here, ρ_i is the level density of three fragments ($i = 1$, 2, and 3). The double integral in the square brackets is the binary convolution integral. The nuclear level density [42,43] is expressed as a function of the fragment excitation energy E_i^* and the single-particle level density parameter a_i:

$$\rho_i(E_i^*) = \frac{1}{12} \left(\frac{\pi^2}{a_i} \right)^{1/4} E_i^{*(-5/4)} \exp(2\sqrt{a_i E_i^*}). \tag{3}$$

In Refs. [18,19], we calculated the excitation energies of the fragments using the single-particle energies of the FRDM [44] at a given temperature, T. In the present work we apply the self-consistent TRMF theory to calculate the excitation energy of the fragments. The excitation energy is calculated as

$$E_i^*(T) = E_i(T) - E_i(T=0). \tag{4}$$

The level density parameter a_i is given as

$$a_i = \frac{E_i^*}{T^2}. \tag{5}$$

In general, the total energy of the parent is more than the sum of the energies of the daughters. The fragment yield in the present calculations can be regarded as the relative fragmentation probability. This relative fragmentation probability (or relative scission point probability) is calculated as the ratio of the probability for a given ternary fragmentation and the sum of the probabilities of all the possible ternary fragmentations and it is given by

$$Y(A_j, Z_j) = \frac{P(A_j, Z_j)}{\sum_j P(A_j, Z_j)}. \tag{6}$$

The competing basic decay modes such as neutron emission, α decay, and binary fragmentation are not considered in the present work. The presented results are the prompt disintegration of a parent nucleus into three fragments (democratic breakup). The resulting excitation energy would be liberated as prompt particle emission or delayed emission, but such secondary emissions are not considered in the present study.

B. RMF formalism

The RMF theories assume that the nucleons interact with each other via the meson fields. The nucleon-meson interaction is given by the Lagrangian density [20–22,24,45,46]:

$$\begin{aligned}\mathcal{L} = {} & \overline{\psi_i}\{i\gamma^\mu\partial_\mu - M\}\psi_i + \frac{1}{2}\partial^\mu\sigma\partial_\mu\sigma - \frac{1}{2}m_\sigma^2\sigma^2 \\ & - \frac{1}{3}g_2\sigma^3 - \frac{1}{4}g_3\sigma^4 - g_\sigma\overline{\psi_i}\psi_i\sigma \\ & - \frac{1}{4}\Omega^{\mu\nu}\Omega_{\mu\nu} + \frac{1}{2}m_w^2V^\mu V_\mu - g_w\overline{\psi}_i\gamma^\mu\psi_i V_\mu \\ & - \frac{1}{4}\vec{B}^{\mu\nu}\cdot\vec{B}_{\mu\nu} + \frac{1}{2}m_\rho^2\vec{R}^\mu\cdot\vec{R}_\mu - g_\rho\overline{\psi}_i\gamma^\mu\vec{\tau}\psi_i\cdot\vec{R}^\mu \\ & - \frac{1}{4}F^{\mu\nu}F_{\mu\nu} - e\overline{\psi}_i\gamma^\mu\frac{(1-\tau_{3i})}{2}\psi_i A_\mu. \end{aligned} \tag{7}$$

Here, ψ_i is the single-particle Dirac spinor. The arrows over the letters in the above equation represent the isovector quantities. The nucleon and the σ-, ω-, and ρ-meson masses are denoted by M, m_σ, m_ω, and m_ρ, respectively. The field for the σ meson is denoted by σ, that for the ω meson by V_μ, and that for the isovector ρ meson by $\vec{R}_\mu$. A_μ denotes the electromagnetic field. $g_\sigma, g_\omega, g_\rho$, and $\frac{e^2}{4\pi}$ are the coupling constants for the σ, ω, and ρ mesons and the photon fields with nucleons, respectively. The strength of the constants g_2 and g_3 is responsible for the nonlinear coupling of the σ mesons (σ^3 and σ^4). The field tensors of the isovector mesons and the photon are given by

$$\Omega^{\mu\nu} = \partial^\mu V^\nu - \partial^\nu V^\mu, \tag{8}$$

$$\vec{B}^{\mu\nu} = \partial^\mu\vec{R}^\nu - \partial^\nu\vec{R}^\mu - g_\rho(\vec{R}^\mu\cdot\vec{R}^\nu), \tag{9}$$

$$F^{\mu\nu} = \partial^\mu A^\nu - \partial^\nu A^\mu. \tag{10}$$

The classical variational principle gives the Euler-Lagrange equation, thus we get the Dirac equation with potential terms for the nucleons and Klein-Gordan equations with source terms for the mesons. We apply the no-sea approximation, so we neglect the antiparticle states. We are dealing with the static nucleus, so the time-reversal symmetry and the conservation of parity simplify the equations. After simplifications, the Dirac equation for the nucleon is given by

$$\{-i\alpha\cdot\nabla + V(r) + \beta[M + S(r)]\}\ \psi_i = \epsilon_i\,\psi_i, \tag{11}$$

where $V(r)$ represents the vector potential and $S(r)$ is the scalar potential,

$$\begin{aligned} V(r) &= g_\omega\omega_0 + g_\rho\tau_3\rho_0(r) + e\frac{(1-\tau_3)}{2}A_0(r), \\ S(r) &= g_\sigma\sigma(r), \end{aligned} \tag{12}$$

which contributes to the effective mass,

$$M^*(r) = M + S(r). \tag{13}$$

The Klein-Gordon equations for the mesons and the electromagnetic fields with the nucleon densities as sources are as follows:

$$\{-\triangle + m_\sigma^2\}\sigma(r) = -g_\sigma\rho_s(r) - g_2\sigma^2(r) - g_3\sigma^3(r), \tag{14}$$

$$\{-\triangle + m_\omega^2\}\omega_0(r) = g_\omega\rho_v(r), \tag{15}$$

$$\{-\triangle + m_\rho^2\}\rho_0(r) = g_\rho\rho_3(r), \tag{16}$$

$$-\triangle A_0(r) = e\rho_c(r). \tag{17}$$

The corresponding densities such as scalar, baryon (vector), isovector, and proton (charge) are given as

$$\rho_s(r) = \sum_i n_i\,\psi_i^\dagger(r)\psi_i(r), \tag{18}$$

$$\rho_v(r) = \sum_i n_i\,\psi_i^\dagger(r)\gamma_0\psi_i(r), \tag{19}$$

$$\rho_3(r) = \sum_i n_i\,\psi_i^\dagger(r)\tau_3\psi_i(r), \tag{20}$$

$$\rho_c(r) = \sum_i n_i\,\psi_i^\dagger(r)\left(\frac{1-\tau_3}{2}\right)\psi_i(r). \tag{21}$$

To solve the Dirac and Klein-Gordan equations, we expand the Boson fields and the Dirac spinor in an axially deformed symmetric harmonic oscillator basis with β_0 as the initial deformation parameter. The nucleon equation along with different meson equations form a set of coupled equations, which can be solved by the iterative method. The center-of-mass correction is calculated with the nonrelativistic approximation $E_{\text{c.m.}} = -3/4\times41A^{-1/3}$. The quadrupole deformation parameter β_2 is calculated from the resulting quadrupole moments of the proton and the neutron. The total energy is

given by [23,47,48]

$$E(T) = \sum_i \epsilon_i n_i + E_\sigma + E_{\sigma\mathrm{NL}} + E_\omega + E_\rho + E_C + E_{\mathrm{pair}} + E_{\mathrm{c.m.}} - AM, \quad (22)$$

with

$$E_\sigma = -\frac{1}{2} g_\sigma \int d^3r \rho_s(r)\sigma(r), \quad (23)$$

$$E_{\sigma\mathrm{NL}} = -\frac{1}{2}\int d^3r \left\{ \frac{2}{3} g_2 \sigma^3(r) + \frac{1}{2} g_3 \sigma^4(r) \right\}, \quad (24)$$

$$E_\omega = -\frac{1}{2} g_\omega \int d^3r \rho_v(r)\omega^0(r), \quad (25)$$

$$E_\rho = -\frac{1}{2} g_\rho \int d^3r \rho_3(r)\rho^0(r), \quad (26)$$

$$E_C = -\frac{e^2}{8\pi} \int d^3r \rho_c(r) A^0(r), \quad (27)$$

$$E_{\mathrm{pair}} = -\triangle \sum_{i>0} u_i v_i = -\frac{\triangle^2}{G}, \quad (28)$$

$$E_{\mathrm{c.m.}} = -\frac{3}{4} \times 41 A^{-1/3}. \quad (29)$$

Here, ϵ_i is the single-particle energy, n_i is the occupation probability, and E_{pair} is the pairing energy obtained from the simple BCS formalism.

C. Pairing and temperature-dependent RMF formalism

Pairing correlation plays a pivotal role in the description of the open shell nuclei and the quantitative description of deformation in heavy nuclei. In the Hartree approximation, we have only the $\psi^\dagger\psi$ (density) term in the Lagrangian. The inclusion of a pairing term like $\psi^\dagger\psi^\dagger$ or $\psi\psi$ and a two-body interaction term like $\psi^\dagger\psi^\dagger\psi\psi$ violates the particle number conservation. So, we apply externally the BCS constant pairing gap approximation for our calculation to take the pairing correlation into account. The pairing interaction energy in terms of the occupation probabilities v_i^2 and $u_i^2 = 1 - v_i^2$ is written as [49,50]

$$E_{\mathrm{pair}} = -G\left[\sum_{i>0} u_i v_i\right]^2, \quad (30)$$

where G is the pairing force constant. The variational approach with respect to the occupation number v_i^2 gives the BCS equation [50]:

$$2\epsilon_i u_i v_i - \triangle\left(u_i^2 - v_i^2\right) = 0, \quad (31)$$

with the pairing gap $\triangle = G\sum_{i>0} u_i v_i$. The pairing gap ($\triangle$) of the proton and the neutron is taken from the empirical formula [23,51]:

$$\triangle = 12 A^{-1/2}. \quad (32)$$

The temperature introduced in the partial occupancies in the BCS approximation is given by

$$n_i = v_i^2 = \frac{1}{2}\left[1 - \frac{\epsilon_i - \lambda}{\tilde{\epsilon}_i}[1 - 2f(\tilde{\epsilon}_i, T)]\right], \quad (33)$$

with

$$f(\tilde{\epsilon}_i, T) = \frac{1}{(1 + \exp[\tilde{\epsilon}_i/T])} \quad \text{and}$$
$$\tilde{\epsilon}_i = \sqrt{(\epsilon_i - \lambda)^2 + \triangle^2}. \quad (34)$$

The function $f(\tilde{\epsilon}_i, T)$ represents the Fermi-Dirac distribution function for quasiparticle energies $\tilde{\epsilon}_i$. The chemical potential λ_p (λ_n) for protons (neutrons) is obtained from the constraints of the particle number equations:

$$\sum_i n_i^Z = Z, \quad \sum_i n_i^N = N. \quad (35)$$

The sum is taken over all proton and neutron states. The entropy is obtained by

$$S = -\sum_i [n_i \ln n_i + (1 - n_i) \ln(1 - n_i)]. \quad (36)$$

The temperature-dependent RMF total energies and the gap parameter are obtained by minimizing the free energy:

$$F = E - TS. \quad (37)$$

In constant pairing gap calculations, for a particular value of pairing gap $\triangle$ and force constant G, the pairing energy E_{pair} diverges, if it is extended to an infinite configuration space. In fact, in all realistic calculations with finite range forces, $\triangle$ is not constant, but decreases with large angular momenta states above the Fermi surface. Therefore, a pairing window in all the equations is extended up to the level $|\epsilon_i - \lambda| \leqslant 2(41A^{-1/3})$ as a function of the single-particle energy. The factor 2 has been determined so as to reproduce the pairing correlation energy for neutrons in ^{118}Sn using Gogny force [23,49,52].

III. RESULTS AND DISCUSSION

In earlier studies [18,19], the level densities of the fragments were calculated using the single-particle energies from the FRDM of Möller *et al.* [53]. The single-particle levels were retrieved from the Reference Input Parameter Library (RIPL-3) [54]. In the present study, we calculate the level densities using the TRMF formalism. We calculate relative fragmentation probabilities for the ternary fragmentation of ^{252}Cf, ^{242}Pu, and ^{236}U with the fixed third fragments $A_3 = {}^{48}$Ca, ^{20}O, and ^{16}O, respectively. The other two fragments with masses and charges A_1, Z_1 and A_2, Z_2 are obtained by keeping the charge-to-mass ratio to be equal to that of parent nucleus as given by Eq. (1). The results are presented for the three different temperatures $T = 1$, 2, and 3 MeV. In principle, one should consider all the possible third fragments. However, in the present study we have neglected such possibilities. From the cluster-decay study of ^{252}Cf [55], it is shown that ^{48}Ca or the neighboring ^{48}Ar or ^{52}Ca has a large preformation probability compared to their light clusters, such as C, O, etc.

In view of experimental data [5] ^{20}O is chosen for ^{242}Pu as the third fragment.

The TRMF equations for the nucleon and the Boson fields are solved within the basis expansion method. In the present work, the numbers of oscillator shells $N_F = 12$ and $N_B = 20$ are used as the basis space for the nucleons and the boson fields, respectively. The total energy is obtained by minimizing the free energy at a given temperature. The ground-state ($T = 0$) binding energies are well reproduced with the experimental data in our calculations.

Ternary system mass distribution and the level densities

Pyatkov *et al.* [6,7] and Oertzen *et al.* [31,56] experimentally observed the heavy third fragments from the new decay mode called collinear cluster tripartition (CCT), in which the ternary fragments are collinearly emitted due to the lower Coulomb interaction for this configuration and at least one of the fragments has the composition with a magic number of nucleons. Further, Pyatkov *et al.* [6] reported that the CCT decay of ^{252}Cf with the ternary ^{48}Ca yields $4.7 \pm 0.2 \times 10^{-3}$/binary fission and the CCT decay of ^{236}U with the ternary ^{34}Si yields $5.1 \pm 0.4 \times 10^{-3}$/binary fission. It was further reported that this yield is due to the whole *Ni-bump* consisting of some hundreds of different mass partitions. In Ref. [7], it is mentioned that the total yield of ^{68,72}Ni ions does not exceed 10^{-4}/binary fission. However, the yield of each separate ternary partition, for instance, ^{128}Sn + ^{72}Ni + ^{52}Ca, can be estimated to be of the order of 3×10^{-6}/binary fission. It is reported that the lighter third fragments like ^{4}He and ^{10}Be have larger yield values in collinear configuration than the clusters like ^{48}Ca and ^{50}Ca [57]. Recently, Balasubramaniam *et al.* [18] studied the ternary fission mass distribution of ^{252}Cf using the FRDM, for the fixed third fragment ^{48}Ca, at temperatures of $T = 1$ and 2 MeV, and revealed Sn + Ni + Ca as the most favorable combination at $T = 2$ MeV. For our investigation, we consider one of the nuclei to be ^{252}Cf for the study of ternary fission at temperatures of $T = 1, 2,$ and 3 MeV. The ternary mass distribution of ^{242}Pu is studied using the third fragment as ^{20}O as suggested by Köster *et al.* [5]. We also studied the ternary fission of ^{236}U for the fixed cluster-like third fragment ^{16}O. For comparison, the ternary fragmentations were also calculated using the FRDM formalism.

The total energy at finite temperature and ground-state energy are calculated using the TRMF formalism as discussed in the Sec. II A. From the TRMF the excitation energy E^* of fragments are calculated using Eq. (4). From the excitation energy E^* and the temperature T the level density parameter a is calculated using Eq. (5). From the excitation energy E^* and the level density parameter a, the level density ρ of fragments are calculated using Eq. (3). From the fragment level densities ρ_i, the folding density ρ_{123} is calculated using the convolution integral Eq. (2) and the relative fragmentation probabilities are calculated using Eq. (6). It is to be noted that the total fragmentation probabilities are normalized to 2 throughout the calculations. In the FRDM formalism, the temperature dependence is introduced in the Fermi occupation number. Using the Lagrange multipliers $\alpha^{N,Z}$ and β and the number equations, the temperature-dependent energy $E(T)$ is calculated from the ground-state single-particle energies for a given temperature, T. The excitation energy E^* at the given temperature is $E^* = E(T) - E(0)$ and other details can be found in Ref. [18].

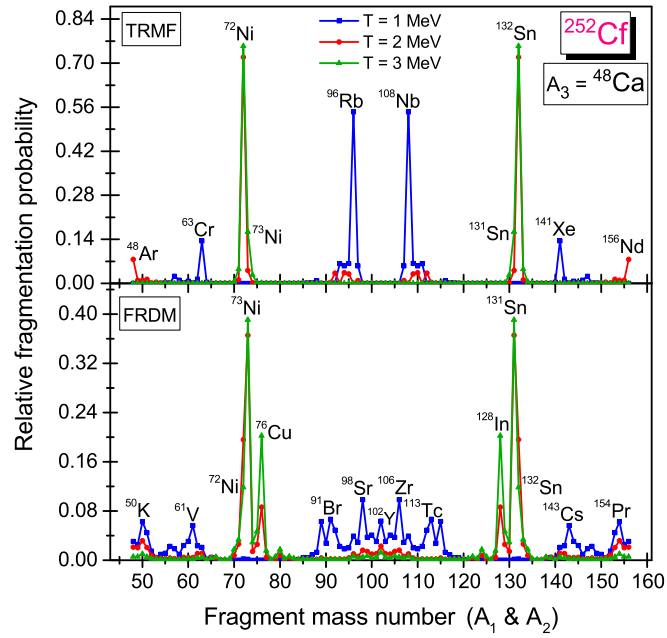

FIG. 1. Ternary fragmentation of ^{252}Cf for the fixed third fragment ^{48}Ca for the temperatures $T = 1$, 2, and 3 MeV. The total fragmentation probabilities are normalized to 2.

In Fig. 1, the TRMF results for the ternary fragmentations of ^{252}Cf for the fixed third fragment ^{48}Ca are shown for

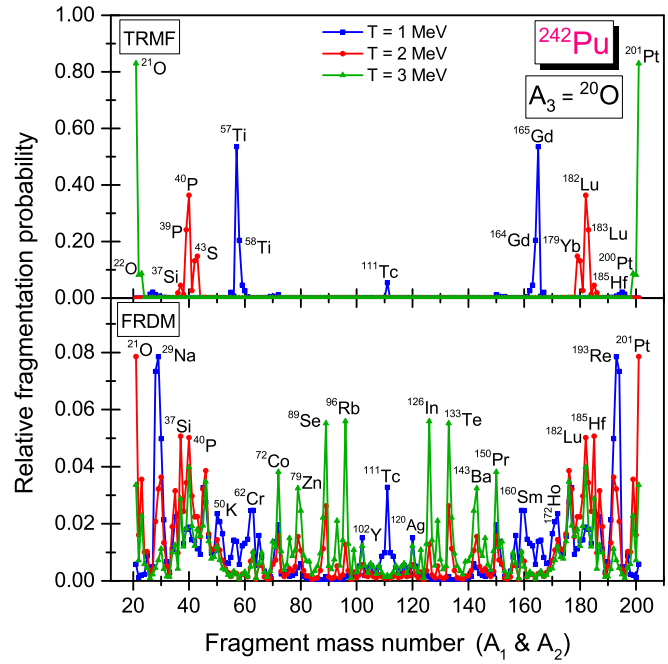

FIG. 2. Ternary fragmentation of ^{242}Pu for the fixed third fragment ^{20}O for the temperatures $T = 1$, 2, and 3 MeV. The total fragmentation probabilities are normalized to 2.

TABLE I. The relative fragmentation probability (RFP) $= Y(A_j, Z_j) = \frac{P(A_j,Z_j)}{\sum P(A_j,Z_j)}$ for ^{252}Cf, ^{242}Pu, and ^{236}U obtained with the TRMF model at temperatures of $T = 1$, 2, and 3 MeV is compared with the FRDM prediction. (The fragmentation probabilities are normalized to 2.)

Parent	T (MeV)	TRMF		FRDM	
		Fragment	RFP	Fragment	RFP
^{252}Cf	1	^{108}Nb + ^{96}Rb + ^{48}Ca	1.090	^{106}Zr + ^{98}Sr + ^{48}Ca	0.196
		^{141}Xe + ^{63}Cr + ^{48}Ca	0.270	^{113}Tc + ^{91}Br + ^{48}Ca	0.134
	2	^{132}Sn + ^{72}Ni + ^{48}Ca	1.438	^{131}Sn + ^{73}Ni + ^{48}Ca	0.732
		^{160}Nd + ^{48}Ar + ^{48}Ca	0.152	^{132}Sn + ^{72}Ni + ^{48}Ca	0.392
	3	^{132}Sn + ^{72}Ni + ^{48}Ca	1.508	^{131}Sn + ^{73}Ni + ^{48}Ca	0.780
		^{131}Sn + ^{73}Ni + ^{48}Ca	0.327	^{128}In + ^{76}Cu + ^{48}Ca	0.404
^{242}Pu	1	^{165}Gd + ^{57}Ti + ^{20}O	1.071	^{193}Re + ^{29}Na + ^{20}O	0.165
		^{164}Gd + ^{58}Ti + ^{20}O	0.409	^{111}Tc + ^{111}Tc + ^{20}O	0.069
	2	^{111}Tc + ^{111}Tc + ^{20}O	0.107	^{160}Sm + ^{62}Cr + ^{20}O	0.052
		^{182}Lu + ^{40}P + ^{20}O	0.726	^{201}Pt + ^{21}O + ^{20}O	0.164
		^{183}Lu + ^{39}P + ^{20}O	0.482	^{185}Hf + ^{37}Si + ^{20}O	0.106
	3	^{179}Yb + ^{43}S + ^{20}O	0.296	^{182}Lu + ^{40}P + ^{20}O	0.106
		^{185}Hf + ^{37}Si + ^{20}O	0.090	^{113}Te + ^{89}Se + ^{20}O	0.056
		^{201}Pt + ^{21}O + ^{20}O	1.660	^{126}In + ^{96}Rb + ^{20}O	0.118
		^{200}Pt + ^{22}O + ^{20}O	0.166	^{133}Te + ^{89}Se + ^{20}O	0.116
^{236}U	1	^{111}Mo + ^{109}Mo + ^{16}O	0.720	^{191}Ta + ^{29}Na + ^{16}O	0.112
		^{161}Pm + ^{59}V + ^{16}O	0.452	^{158}Nd + ^{62}Cr + ^{16}O	0.084
	2	^{110}Mo + ^{110}Mo + ^{16}O	0.395	^{180}Tm + ^{40}P + ^{16}O	0.058
		^{180}Tm + ^{40}P + ^{16}O	0.794	^{131}Sn + ^{89}Se + ^{16}O	0.468
		^{181}Tm + ^{39}P + ^{16}O	0.554	^{130}In + ^{90}Br + ^{16}O	0.230
	3	^{177}Er + ^{43}S + ^{16}O	0.166	^{180}Tm + ^{40}P + ^{16}O	0.064
		^{183}Yb + ^{37}Si + ^{16}O	0.136	^{199}Os + ^{21}O + ^{16}O	0.046
		^{199}Os + ^{21}O + ^{16}O	1.174	^{131}Sn + ^{89}Se + ^{16}O	0.458
		^{197}Os + ^{23}O + ^{16}O	0.432	^{130}Sn + ^{90}Br + ^{16}O	0.312
		^{132}Sn + ^{88}Se + ^{16}O	0.136	^{132}Sn + ^{88}Se + ^{16}O	0.188

different temperatures. For $T = 1$ MeV, ^{108}Nb + ^{96}Rb + ^{48}Ca is the most probable fragmentation followed by ^{141}Xe + ^{63}Cr + ^{48}Ca. For higher temperatures $T = 2$ and 3 MeV, it is interesting to see that ^{132}Sn + ^{72}Ni + ^{48}Ca is the most favorable combination of the existing fragmentations.

In Figs. 2 and 3, we display the TRMF results for the ternary fragmentations of ^{242}Pu and ^{236}U for the fixed third fragments ^{20}O and ^{16}O, respectively. At $T = 1$ MeV, we see both symmetric and asymmetric fragmentation for ^{242}Pu and ^{236}U. For ^{242}Pu, at $T = 1$ MeV, ^{165}Gd + ^{57}Ti + ^{20}O is the most favorable combination rather than the symmetric binary fragments ^{111}Tc + ^{111}Tc + ^{20}O. For $T = 2$ MeV, ^{182,183}Lu + ^{40,39}P + ^{20}O, ^{179}Yb + ^{43}S + ^{20}O, and ^{185}Hf + ^{37}Si + ^{20}O are the possible relative fragmentation probabilities. At $T = 3$ MeV ^{201}Pt + ^{21}O + ^{20}O is the most favorable fragmentation. For ^{236}U, at $T = 1$ MeV, the symmetric breakup into the heavy fragments ^{109}Mo + ^{111}Mo and ^{110}Mo + ^{110}Mo along with the third fragment ^{16}O has larger scission point probabilities. In addition, the fragment combinations ^{161}Pm + ^{59}V + ^{16}O and ^{163}Sm + ^{57}Ti + ^{16}O also have larger fragmentation probabilities. For $T = 2$ MeV, ^{180,181}Tm + ^{40,39}P + ^{16}O are the most probable fragments. Further, ^{177}Er + ^{43}S + ^{16}O and ^{183}Yb + ^{37}Si + ^{16}O are also the probable ternary fragments. It is seen that, at $T = 3$ MeV, the fragments ^{199,198,197}Os + ^{21,22,23}O + ^{16}O have considerable scission point probabilities. In Ref. [19], it is predicted that the ternary charge distribution of ^{252}Cf, at $T = 2$ MeV, with Si, P, and S as the most favorable fragments along with Sn and the corresponding partner. Here, at $T = 3$ MeV, the most favorable fragment is one of the closed shell ($Z = 8$) nuclei. Although, one would expect the even-even fragments as more probable for fission, we find a large number of odd-mass fragments possessing maximum fragmentation probability compared to even-even fragments. This is due to the fact that the level densities of the odd-mass fragments are higher than those of the even-mass fragments as reported in Ref. [41].

For comparison, in Figs. 1–3, the FRDM results for the ternary fragmentations are also presented. For quick reference, the most probable ternary fragmentations and their relative scission point probabilities are tabulated in Table I at three different temperatures: $T = 1, 2$, and 3 MeV. In general, at $T = 1$ MeV, the most favorable fragments of the FRDM formalism are quite different than those for the TRMF formalism. These differences may be attributed to the differences in the excitation energies obtained in the TRMF and FRDM formalisms. For ^{252}Cf, the TRMF and FRDM results agree qualitatively with each other at $T = 2$ and 3 MeV. For ^{242}Pu, more fragments have considerable fragmentation probabilities in the FRDM formalism. At $T = 2$ and 3 MeV, the favorable fragmentations are in the mass range $A_1 \sim 180$ and 130 region with their corresponding partners. The TRMF and FRDM results agree only partially for the ^{242}Pu nucleus at $T = 2$ MeV. For ^{236}U,

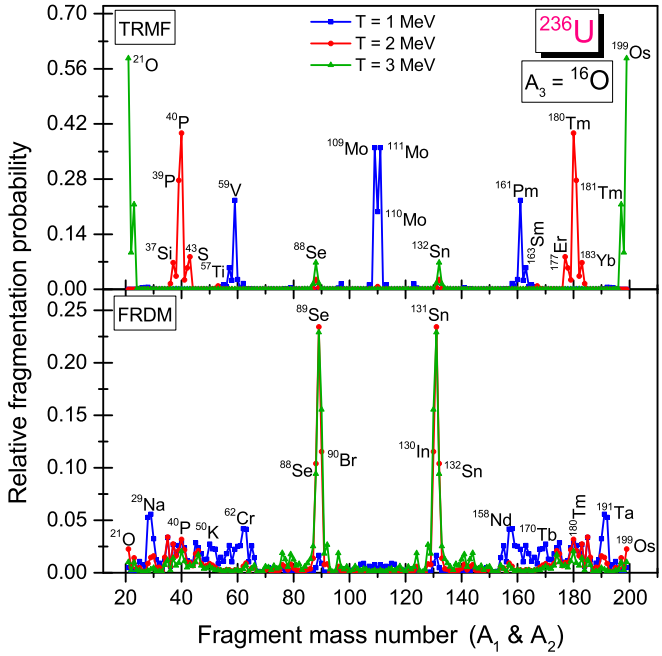

FIG. 3. Ternary fragmentation of ^{236}U for the fixed third fragment ^{16}O for the temperatures $T = 1, 2$, and 3 MeV. The total fragmentation probabilities are normalized to 2.

the most favorable fragments are at $A_1 \sim 130$ for $T = 2$ and 3 MeV in FRDM calculations. One of the favorable fragments has a closed shell nucleon or a near closed shell ($N = 82$) nucleus. Further, in both the formalisms, at $T = 2$ MeV, we get nearly similar fragments such as ^{40}P along with their partners ^{180}Tm and ^{16}O as shown in Fig. 3. The doubly closed shell nucleus ^{132}Sn is appears in both the cases, at $T = 3$ MeV.

To illustrate the difference between the TRMF and FRDM results, we studied the level density parameter a, which is a

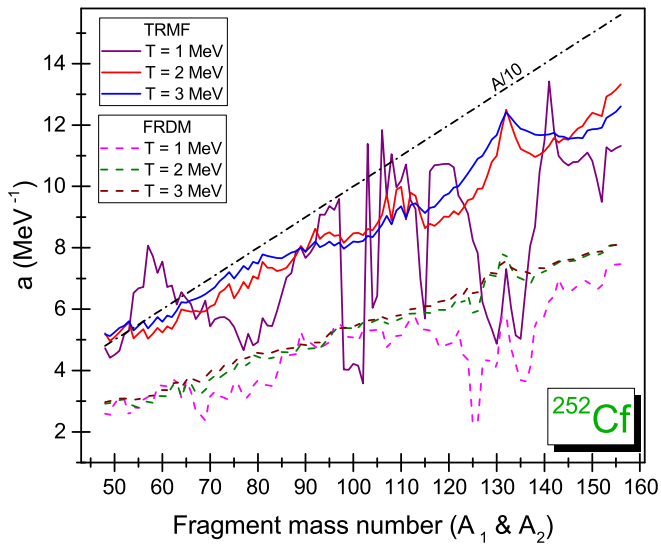

FIG. 4. The level density parameter a of the ternary fragmentation of ^{252}Cf for the temperatures $T = 1, 2$, and 3 MeV within the TRMF and FRDM formalisms.

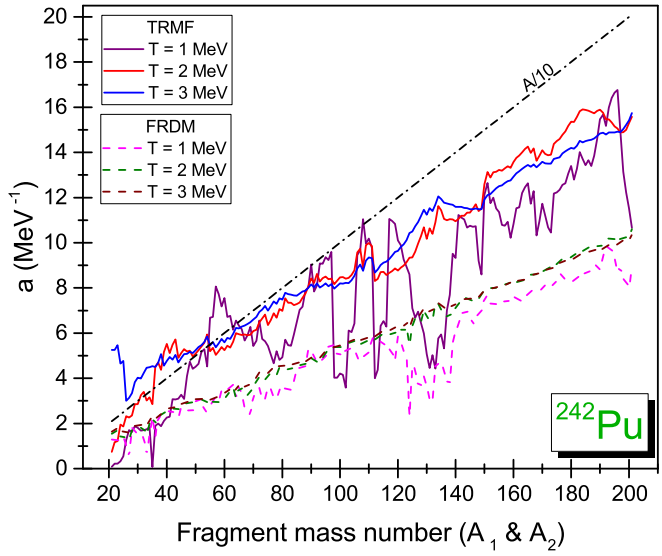

FIG. 5. The level density parameter a of the ternary fragmentation of ^{242}Pu for the temperatures $T = 1, 2$, and 3 MeV within the TRMF and FRDM formalisms.

crucial quantity. In general, the level density parameter a is given by the empirical estimation relation [58]:

$$a = \frac{A}{K}(\text{MeV}^{-1}), \tag{38}$$

where K is the inverse level density parameter and varies from 10 to 14 depending on the mass number A of the nucleus. In Figs. 4–6, we have plotted the level density parameter a of the fission fragments for ^{252}Cf, ^{242}Pu, and ^{236}U as a function of mass number. Here, we consider the inverse level density parameter $K = 10$ (which is quite a practical value as mentioned in Ref. [58]) for all nuclei, which is shown in the

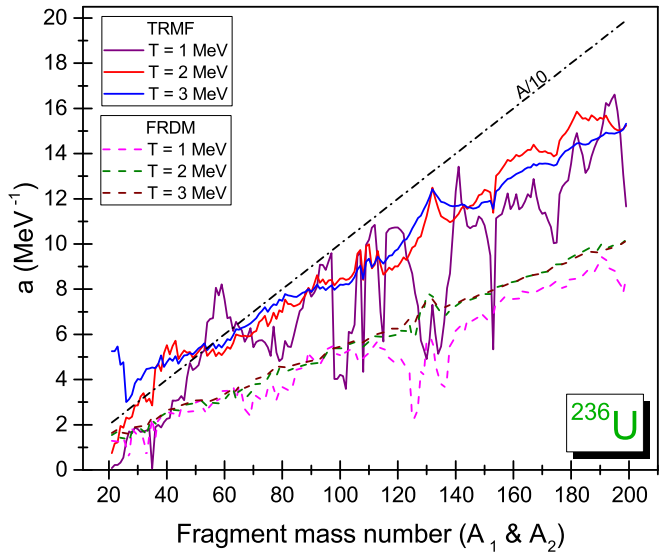

FIG. 6. The level density parameter a of the ternary fragmentation of ^{236}U for the temperatures $T = 1, 2$, and 3 MeV within the TRMF and FRDM formalisms.

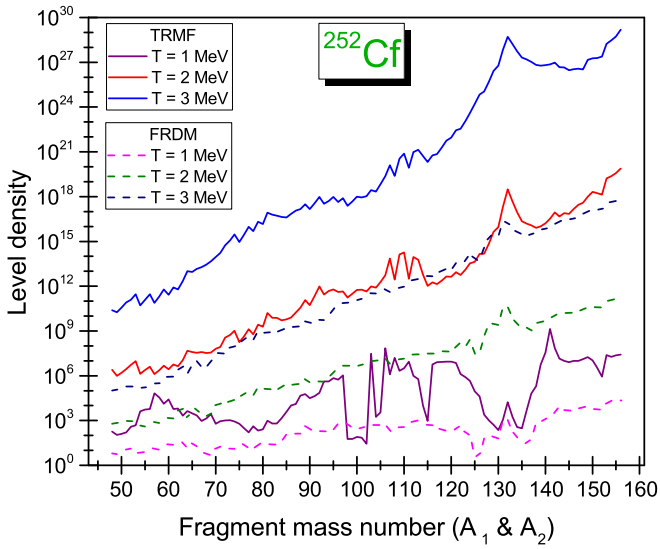

FIG. 7. The level density of the ternary fragmentation of ^{252}Cf for the temperatures $T = 1$, 2, and 3 MeV.

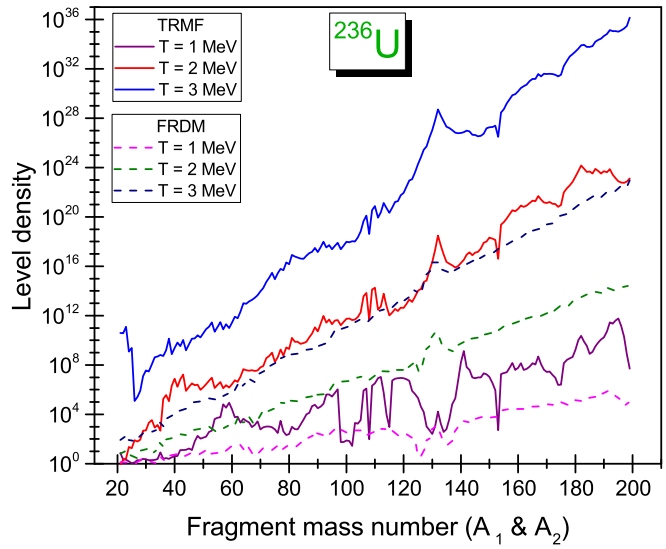

FIG. 9. The level density of the ternary fragmentation of ^{236}U for the temperatures $T = 1$, 2, and 3 MeV.

plots as a black dashed-dotted line. From these figures, one can see that the TRMF values are very near to the empirical level density parameter a. The FRDM values are considerably lower than the referenced level density parameter. Further, in both models at $T = 1$ MeV, there are more fluctuations in a due to the shell effects of the fission fragments. For ^{252}Cf and ^{236}U, the level density parameter a promptly increases for the doubly closed shell nucleus ^{132}Sn and has the lowest inverse level density parameter $K = 10.9$. For ^{242}Pu, the ^{132}Sn nucleus was restricted by Eq. (1). However, value of parameter a increases towards the neutron closed shell ($N = 82$) nuclei. In the TRMF model the prompt increase of the level density towards the doubly closed shell nucleus ^{132}Sn is clearly seen at $T = 3$ MeV due to the fact all fission fragments become a spherical Fermi liquid drop.

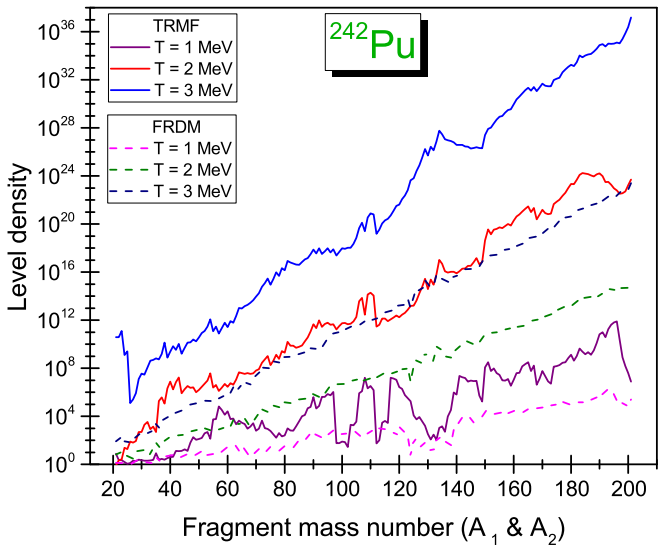

FIG. 8. The level density of the ternary fragmentation of ^{242}Pu for the temperatures $T = 1$, 2, and 3 MeV.

To understand the results better we have plotted the level density of the fragments (A_2 and A_1) of the heavy nuclei ^{252}Cf, ^{242}Pu, and ^{236}U as a function of mass number as shown in Figs. 7–9. From Fig. 7, it can be seen that for $T = 2$ and 3 MeV, the level density of ^{132}Sn is higher than that for the neighboring nuclei in both formalisms. Hence, ^{132}Sn becomes the most favorable fragment. Figure 9 shows, once again, that ^{132}Sn has a level density higher than that of the neighboring nuclei; however, the corresponding partner has lower or nearly the same level density as the neighboring nuclei in the TRMF model. For the nucleus ^{242}Pu, ^{132}Sn is restricted due to the charge-to-mass ratio. From Figs. 8 and 9, we see that the fragments Si to S have large level densities compared with the neighboring nucleus and the corresponding partners also have similar behavior. At $T = 3$ MeV, the light-charged particles, $Z_2 = 8$, have a level density larger than that of the neighboring nuclei and its corresponding partners also have similar behavior. In the FRDM formalism, the level density of the doubly closed shell nuclei ^{132}Sn has a larger value than the neighboring nuclei for ^{252}Cf and ^{236}U at $T = 2$ and 3 MeV. For ^{242}Pu, there is no prompt increase in the level density due to the restricted fragment ^{132}Sn by Eq. (1).

Further, from Figs. 7 and 9, it can be seen that the level density promptly increases while reaching the doubly closed shell nucleus ^{132}Sn in both formalisms. It is noted that, other than the light-charged particles, ^{132}Sn has the larger level density. This indicates that, the ternary combinations with larger phase spaces become more probable than the other ternary combinations.

IV. SUMMARY AND CONCLUSIONS

We have studied the ternary fragmentation of ^{252}Cf, ^{242}Pu, and ^{236}U nuclei within statistical theory. Various inputs to statistical theory, like the excitation energies and the level density parameters for the different fission fragments at a given temperature, are calculated from the TRMF model. The

ternary combinations for these nuclei are obtained from the charge-to-mass ratio of the parent nuclei. For the comparison, the results obtained using the FRDM inputs to statistical theory are also presented.

For the nucleus ^{252}Cf we obtained Sn + Ni + Ca as the most probable ternary combination at the temperatures $T = 2$ and 3 MeV. For the nuclei ^{242}Pu and ^{236}U, however, we obtained a few different fragmentations at $T = 2$ and 3 MeV. For these nuclei, at $T = 2$ MeV, Si, P, and S are the possible ternary fragments along with the corresponding fragments. For $T = 3$ MeV, the oxygen isotopes have the larger fragmentation probabilities. The TRMF results for ^{252}Cf at $T = 2$ and 3 MeV resemble very well those for the FRDM, whereas they are strikingly differ from each other at $T = 1$ MeV. In the case of ^{236}U, the ternary fission fragments corresponding to the TRMF model and the FRDM resemble each other only at $T = 3$ MeV. For ^{242}Pu, the ternary fragmentations for the TRMF model and the FRDM are by and large at variance at all the temperatures considered. Thus, it seems that the ternary fragmentations are quite sensitive to the thermal evolution of the deformation and the single-particle energies as they affect the excitation energy and the level density parameter. These aspects are treated self-consistently within the TRMF model, while being ignored within the later approach.

ACKNOWLEDGMENTS

M.T.S. acknowledges the financial support from the UGC-BSR (Grant No. F.25-1/2014-15(BSR)7-307/2010/(BSR), dated 05.11.2015) and the IOP, Bhubhaneswar, for the warm hospitality and for providing the necessary computer facilities.

[1] R. D. Present and J. K. Knipp, Phys. Rev. **57**, 751 (1940).
[2] T. San-Tsiang, H. Zah-Vei, L. Vigneron, and R. Chastel, Nature (London) **159**, 773 (1947).
[3] M. L. Muga, C. R. Rice, and W. A. Sedlacek, Phys. Rev. **161**, 1266 (1967).
[4] A. V. Ramayya, J. K. Hwang, J. H. Hamilton, A. Sandulescu, A. Florescu, G. M. Ter-Akopian, A. V. Daniel, Y. T. Oganessian, G. S. Popeko, W. Greiner, and J. D. Cole (GANDS95 Collaboration), Phys. Rev. Lett. **81**, 947 (1998); A. V. Ramayya, Phys. Rev. C **57**, 2370 (1998).
[5] U. Köster, H. Faust, G. Fioni, T. Friedrichs, M. Groß, and S. Oberstedt, Nucl. Phys. A **652**, 371 (1999).
[6] Y. V. Pyatkov *et al.*, Eur. Phys. J. A **45**, 29 (2010).
[7] Y. V. Pyatkov *et al.*, Eur. Phys. J. A **48**, 94 (2010).
[8] P. Fong, Phys. Rev. C **3**, 2025 (1971).
[9] H. Diehl and W. Greiner, Nucl. Phys. A **229**, 29 (1974).
[10] V. A. Rubchenya and S. G. Yavshits, Z. Phys. A: At. Nucl. **329**, 217 (1988).
[11] W. von Oertzen and A. K. Nasirov, Phys. Lett. B **734**, 234 (2014).
[12] K. Manimaran and M. Balasubramaniam, Phys. Rev. C **79**, 024610 (2009).
[13] K. R. Vijayaraghavan, M. Balasubramaniam, and W. von Oertzen, Phys. Rev. C **90**, 024601 (2014).
[14] A. V. Karpov, Phys. Rev. C **94**, 064615 (2016).
[15] K. R. Vijayaraghavan, M. Balasubramaniam, and W. von Oertzen, Eur. Phys. J. A **48**, 27 (2012).
[16] P. Holmvall, U. Köster, A. Heinz, and T. Nilsson, Phys. Rev. C **95**, 014602 (2017).
[17] M. Rajasekaran and V. Devanathan, Phys. Rev. C **24**, 2606 (1981).
[18] M. Balasubramaniam, C. Karthikraj, S. Selvaraj, and N. Arunachalam, Phys. Rev. C **90**, 054611 (2014).
[19] M. T. Senthil Kannan and M. Balasubramaniam, Eur. Phys. J A (to be published) (2017).
[20] J. D. Walecka, Ann. Phys. **83**, 491 (1974).
[21] C. J. Horowitz and B. D. Serot, Nucl. Phys. A **368**, 503 (1981).
[22] B. D. Serot and J. D. Walecka, in *Advances in Nuclear Physics 16*, edited by J. W. Negele and E. Vogt (Plenum Press, New York, 1986), p. 1.
[23] Y. K. Gambhir, P. Ring, and A. Thimet, Ann. Phys. **198**, 132 (1990).
[24] S. K. Patra and C. R. Praharaj, Phys. Rev. C **44**, 2552 (1991).
[25] Y. K. Gambhir, J. P. Maharana, G. A. Lalazissis, C. P. Panos, and P. Ring, Phys. Rev. C **62**, 054610 (2000).
[26] B. K. Agrawal, T. Sil, J. N. De, and S. K. Samaddar, Phys. Rev. C **62**, 044307 (2000); **63**, 024002 (2001).
[27] T. Sil, B. K. Agrawal, J. N. De, and S. K. Samaddar, Phys. Rev. C **63**, 064302 (2001).
[28] P. Arumugam, B. K. Sharma, S. K. Patra, and R. K. Gupta, Phys. Rev. C **71**, 064308 (2005).
[29] B. K. Sharma, P. Arumugam, S. K. Patra, P. D. Stevenson, R. K. Gupta, and W. Greiner, J. Phys. G **32**, L1 (2006).
[30] S. K. Patra, R. K. Gupta, B. K. Sharma, P. D. Stevenson, and W. Greiner, J. Phys. G **34**, 2073 (2007).
[31] W. von Oertzen *et al.*, Eur. Phys. J. A **36**, 279 (2008).
[32] R. K. Gupta, S. K. Patra, P. D. Stevenson, C. Beck, and W. Greiner, J. Phys. G **35**, 075106 (2008).
[33] K. Rutz, J. A. Maruhn, P.-G. Reinhard, and W. Greiner, Nucl. Phys. A **590**, 680 (1995).
[34] S. K. Patra, R. K. Choudhury, and L. Satpathy, J. Phys. G **37**, 085103 (2010).
[35] B. Singh, B. B. Sahu, and S. K. Patra, Phys. Rev. C **83**, 064601 (2011).
[36] B. Singh, M. Bhuyan, S. K. Patra, and R. K. Gupta, J. Phys. G **39**, 025101 (2012).
[37] B. B. Sahu, S. K. Singh, M. Bhuyan, S. K. Biswal, and S. K. Patra, Phys. Rev. C **89**, 034614 (2014).
[38] B. Kumar, S. K. Singh, and S. K. Patra, Int. J. Mod. Phys. **24**, 1550017 (2015).
[39] B. Kumar, S. K. Biswal, S. K. Singh, and S. K. Patra, Phys. Rev. C **92**, 054314 (2015).
[40] G. A. Lalazissis, J. König, and P. Ring, Phys. Rev. C **55**, 540 (1997).
[41] P. Fong, Phys. Rev. **102**, 434 (1956).
[42] J. R. Huizenga and L. G. Moretto, Annu. Rev. Nucl. Sci. **22**, 427 (1972).
[43] H. Bethe, Rev. Mod. Phys. **9**, 69 (1937).
[44] P. Möller, J. R. Nix, W. D. Myers, and W. J. Swiatecki, At. Data Nucl. Data Tables **66**, 131 (1997).
[45] J. Boguta and A. R. Bodmer, Nucl. Phys. A **292**, 413 (1977).
[46] C. E. Price and G. E. Walker, Phys. Rev. C **36**, 354 (1987).
[47] P. G. Blunden and M. J. Iqbal, Phys. Lett. B **196**, 295 (1987).
[48] P. G. Reinhard, Rep. Prog. Phys. **52**, 439 (1989).

[49] S. K. Patra, Phys. Rev. C **48**, 1449 (1993).
[50] M. A. Preston and R. K. Bhaduri, in *Structure of the Nucleus* (Addison-Wesley, Reading, MA, 1982), Chap 8, p. 309.
[51] D. Vautherin, Phys. Rev. C **7**, 296 (1973).
[52] J. Dechargé and D. Gogny, Phys. Rev. C **21**, 1568 (1980).
[53] P. Möller, J. R. Nix, and K. L. Kratz, At. Data Nucl. Data Tables **59**, 185 (1995).
[54] https://www-nds.iaea.org/RIPL-3/
[55] M. Balasubramaniam and R. K. Gupta, Phys. Rev. C **60**, 064316 (1999).
[56] W. von Oertzen, V. Zherebchevsky, B. Gebauer, C. Schulz, S. Thummerer, D. Kamanin, G. Royer, and T. Wilpert, Phys. Rev. C **78**, 044615 (2008).
[57] K. Manimaran and M. Balasubramaniam, Phys. Rev. C **83**, 034609 (2011).
[58] B. Nerlo-Pomorska, K. Pomorski, J. Bartel, and K. Dietrich, Phys. Rev. C **66**, 051302(R) (2002).